Electronic Supplementary Material (ESI) for Journal of Materials Chemistry A.

Supporting Information

Zn^{2+} ion doping for structural modulation of lead-free Sn-based perovskite solar cells

Hyungsu Jang,[a] Hyeong Yong Lim,[a] Chan Beom Park,[a] Jongdeuk Seo,[a] Jung Geon Son,[a] Taehee Song,[a] Jaehwi Lee,[a] Yun Seop Shin,[a] Jina Roe,[a] Sang Kyu Kwak,*[c] Dong Suk Kim*[b] and Jin Young Kim,*[ab]

a. School of Energy and Chemical Engineering, Ulsan National Institute of Science and Technology (UNIST), Ulsan 44919, Republic of Korea.

b. Graduate School of Carbon Neutrality, Ulsan National Institute of Science and Technology (UNIST), Ulsan 44919, Republic of Korea.

c. Department of Chemical and Biological Engineering, Korea University, 145 Anam-ro, Seongbuk-gu, Seoul 02841, Republic of Korea.

*Correspondence author. E-mail: skkwak@korea.ac.kr (S. K. K.), kimds@unist.ac.kr (D. S. K), jykim@unist.ac.kr (J. Y. K)

Experimental Procedures

Materials

N,N-dimethylformamide (DMF, anhydrous, 99.8%), dimethyl sulfoxide (DMSO, anhydrous, 99.5%), chlorobenzene (CB, anhydrous 99.8%), tin (II) iodide (SnI_2, 99.99%), tin (II) fluoride (SnF_2, 99%), Ethane-1,2-diammonium iodide ($EDAI_2$, 98%) and zinc powder (Zn^0, 99.9%) were purchased from Sigma-Aldrich. Formamidinium iodide (FAI, 99.99%) was purchased from Greatcell Solar Materials. Poly(3,4-ethylenedioxythiophene) polystyrene sulfonate (PEDOT:PSS, Clevios PVP AI 4083) was purchased from Heraeus. C_{60} (99.95%) was purchased from Materials Technologies Research (MTR Ltd.). Bathocuproine (BCP, purified by sublimation, 99%) was purchased from TCI.

Device fabrication

ITO-coated glass substrates were cleaned by ultra-sonication in deionized water, acetone, and isopropyl alcohol for 10 min each. A poly(3,4-ethylenedioxythiophene): polystyrene sulfonic acid (PEDOT:PSS) layer was deposited on the ITO substrates by spin-coating at 5000 rpm for 30 s, followed by annealing at 150 °C for 20 min. The 0.9M pristine perovskite precursor solution was prepared by 0.98:0.01:1:0.1 molar ratio of FAI, $EDAI_2$, SnI_2, and SnF_2 dissolved in DMF and DMSO (4:1 v/v%) co-solvent. Then the Zn-doped precursor solution was prepared by adding different mole fractions of Zn^0 powder (2%, 5%, 10%) with pristine precursor. The perovskite precursor was coated onto the PEDOT:PSS/ITO substrate by a spin-coating process at 5000 rpm for 40 s. After 10 s, the perovskite film was treated with chlorobenzene drop-casting. The substrate was dried on a hot plate at 70 °C for 15 min. Deposition of the Sn-perovskite films was performed in an N_2 glove box. Subsequently, C_{60} (20 nm), BCP (5 nm), Ag (100 nm) are sequentially evaporated by thermal evaporation under vacuum ($<10^{-6}$ Torr).

Characterizations

XRD patterns were obtained by using a high-power diffractometer (D/MAX2500V/PC from Rigaku) with settings including 40 kV potential, 200 mA current, Cu-rotating anode, and Cu Kα radiation ($\lambda = 0.1542$ nm). The GIXRD patterns were obtained by using a high-resolution diffractometer (D8 DISCOVERY, Brucker). SEM was performed using an S-4800 Hitachi High-Technology microscope. Grain size distribution and pinhole counts from the SEM image were obtained by using ImageJ software (U.S. National Institutes of Health, https://imagej.nih.gov/ij/). UV-Vis-NIR absorption spectra were obtained by using a Cary 5000

(Agilent) spectrophotometer and photoluminescence spectra were measured with an nF900 instrument (Edinburgh Photonics) with a xenon lamp as an excitation source. TRPL measurements were conducted using PicoQuant FluoTime 300 (PicoQuant GmbH, Germany) equipped with a PDL 820 laser pulse driver. A pulsed laser diode (λ = 375 nm, pulse FWHM < 70 ps, repetition rate 200 kHz-40 MHz) was used to excite the sample. XPS and UPS measurements were conducted with ESCALAB 250XI. The *J-V* characteristics were collected with a Keithley 2635 A source measurement unit inside the N_2-filled glove box using a high-quality optical fiber to guide the light from a solar simulator to the device. Light intensity was calibrated with a KG5-filtered Si reference cell calibrated from National Renewable Energy Laboratory (NREL). External quantum efficiency (EQE) measurements were performed using a QUANTX-300 (Newport Co.).

Density functional theory calculation.

We have performed the density functional theory (DFT) calculation to investigate the effect of the Zn doping on the thermodynamic stability and the structure of $FASnI_3$ using the Cambridge Serial Total Energy Package (CASTEP).[1] All calculations were performed using the generalized gradient approximation (GGA) with the Perdew-Burke-Emzerhof (PBE) functional and spin polarization was included.[2, 3] The on-the-fly generation (OTFG) ultrasoft pseudopotential was employed to describe the interactions between the core and the valence electrons and the energy cutoff was set to 517 eV.[4] The convergence criterion for the geometry optimization and SCF convergence were 1×10^{-5} eV/atom and 1×10^{-6} eV/atom, respectively. The convergence tolerance of ionic relaxation for maximum force, stress and displacement was 0.03 eV/Å, 0.05 GPa, and 0.001 Å, respectively. The van der Waals interactions were modelled with the Tkatchenko-Scheffler (TS) method.[5] The geometry optimization of bulk systems with the angles fixed was done applying the two-point steepest descent (TPSD) algorithm.[6] The *k*-point separation was set as 0.04 $Å^{-1}$ in the Brillouin zone for all calculations.[7] For modeling $FASnI_3$ doped with Zn, $3 \times 3 \times 3$ supercells were constructed and 1, 2, 3, and 4 Sn atoms were replaced to obtain 3.70, 7.4, 11.1, and 14.7 at.% Zn-doped $FASnI_3$, repectively (Figure SX2a). Considering various doping configurations, we selected structures for each Zn doping concentration with the lowest enthalpy of formation (Figure SX2b, c).

To evaluate the thermodynamic stability of Zn doped $FASnI_3$, the enthalpy of formation of $FASnI_3$ are computed. It is known that $FASnI_3$ decomposes into FAI and SnI_2,[8] so we calculated the enthalpy of formation (ΔH) for the pristine $FASnI_3$ and Zn-doped $FASnI_3$ as follows,

$$\Delta H = E\left[FAZn_xSn_{1-x}I_3\right] - E[FAI] - (1-x)E\left[SnI_2\right] - xE\left[I_2\right] - xE[Zn] \quad \text{(X1)}$$

In the above equation, x represents the at. % of Zn in the perovskite structure and *E* is the total energy of the optimized structures.

The volume changes, ΔV, is calculated as follows,

$$\Delta V = \frac{V_{Zn-doped} - V_{pristine}}{V_{pristine}} \times 100\ (\%) \quad \text{(X2)}$$

where $V_{Zn-doped}$ and $V_{pristine}$ are volume of Zn-doped and pristine $FASnI_3$ supercells, respectively, used in the calculations.

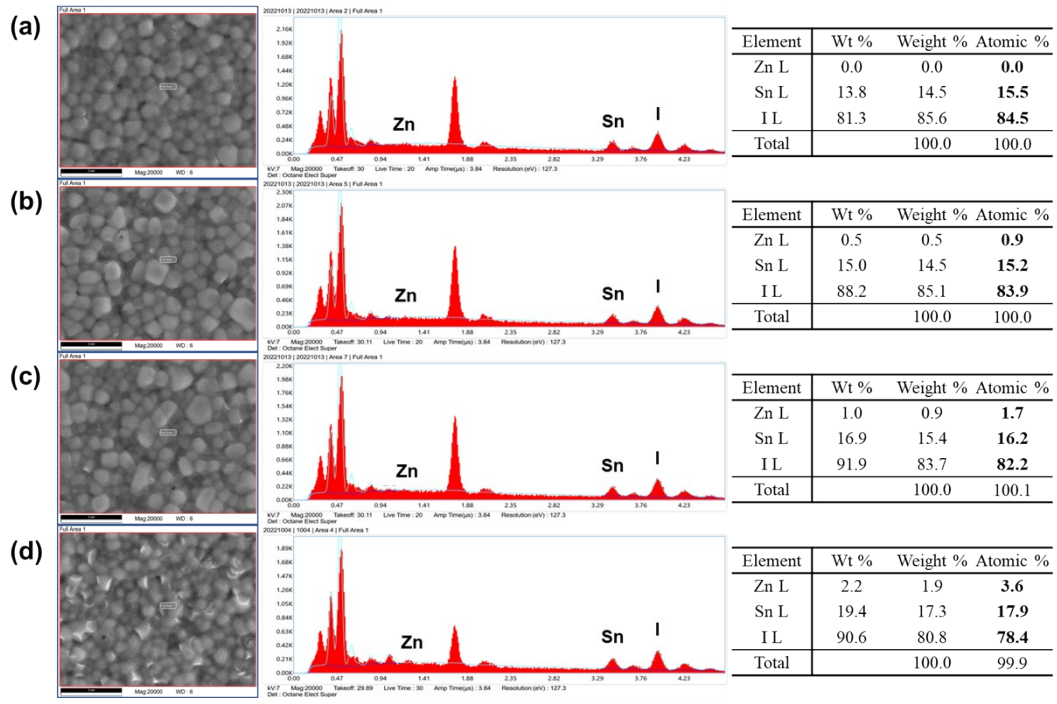

(a)

Element	Wt %	Weight %	Atomic %
Zn L	0.0	0.0	**0.0**
Sn L	13.8	14.5	**15.5**
I L	81.3	85.6	**84.5**
Total		100.0	100.0

(b)

Element	Wt %	Weight %	Atomic %
Zn L	0.5	0.5	**0.9**
Sn L	15.0	14.5	**15.2**
I L	88.2	85.1	**83.9**
Total		100.0	100.0

(c)

Element	Wt %	Weight %	Atomic %
Zn L	1.0	0.9	**1.7**
Sn L	16.9	15.4	**16.2**
I L	91.9	83.7	**82.2**
Total		100.0	100.1

(d)

Element	Wt %	Weight %	Atomic %
Zn L	2.2	1.9	**3.6**
Sn L	19.4	17.3	**17.9**
I L	90.6	80.8	**78.4**
Total		100.0	99.9

Figure S1. Energy dispersive X-ray spectroscopy (EDS) spectra of perovskite films. The energy spectrum and measured atomic percentages of the main elements (Zn, Sn, I) in the perovskite are summarized in tables. Zn component can be calculated to 0.0 %, 0.9 %, 1.7 %, and 3.6 % in the control (a), Zn-2 (b), Zn-5 (c), and Zn-10 (d) perovskite films, respectively.

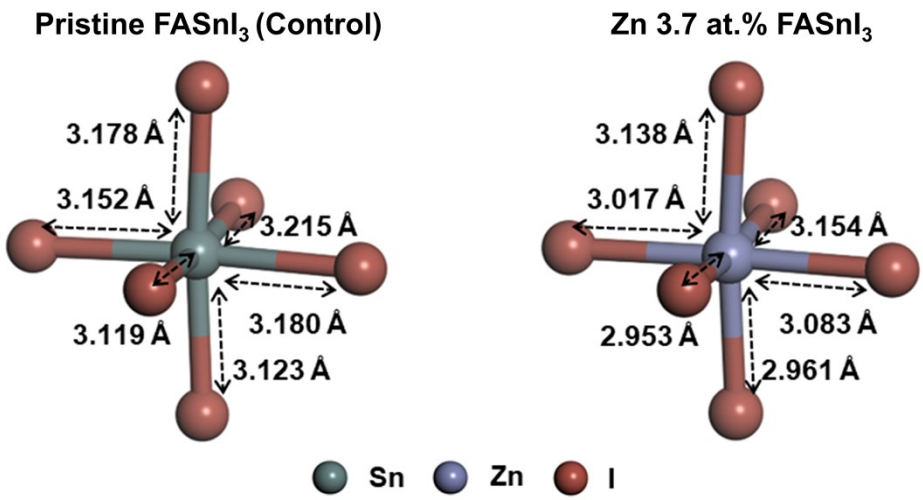

Figure S2. Schematics of the bond length for pristine $FASnI_3$ (control) and 3.7 at. % Zn doped $FASnI_3$.

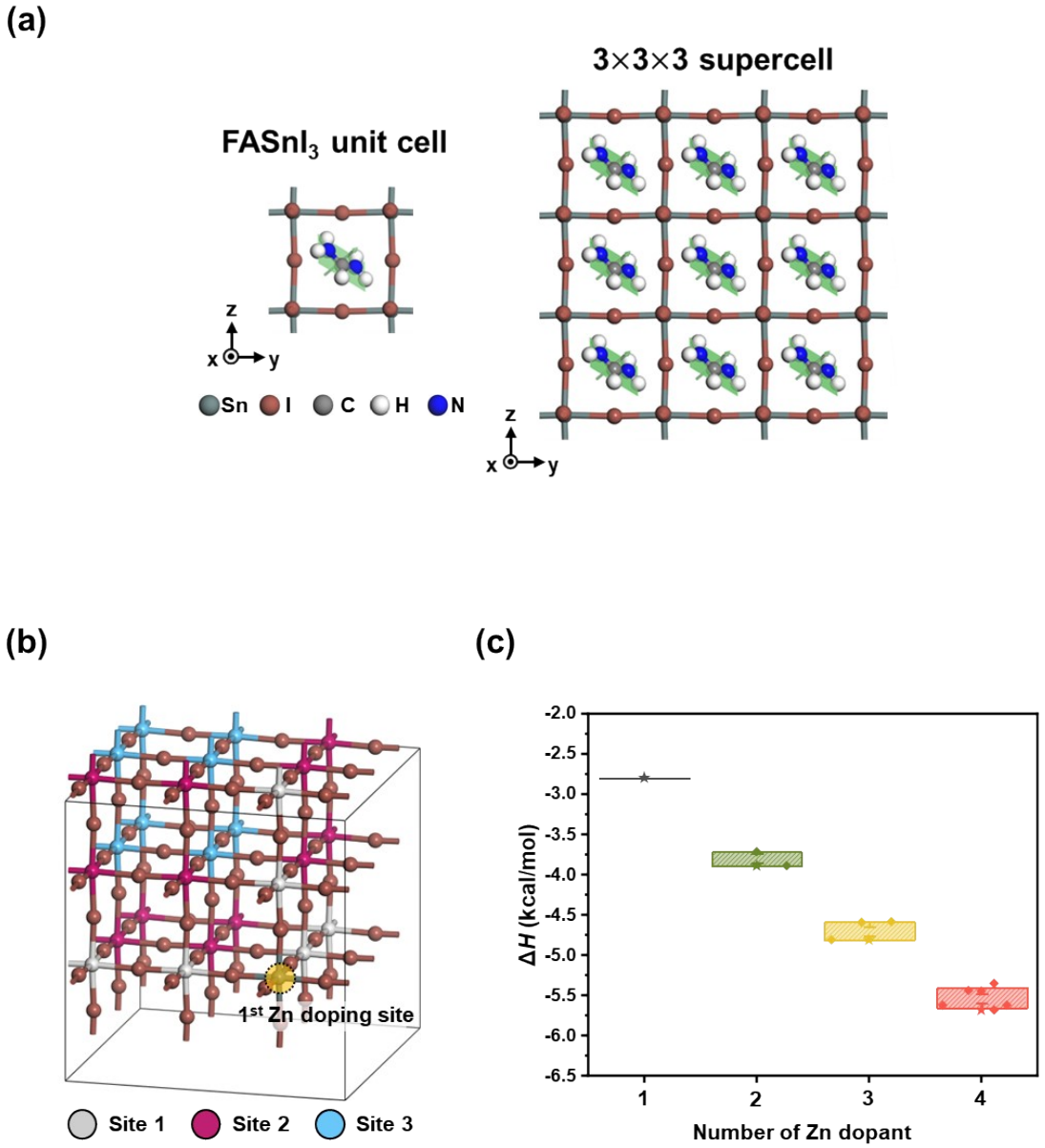

Figure S3. (a) Unit cell structures and $3 \times 3 \times 3$ supercell of $FASnI_3$. (b) Zn doping sites considered in DFT calculations. The possible doping sites were colored with silver (site 1), violet (site 2), and light blue (site 3) depending on the distance centered on the yellow-shaded circle considering the periodicity. We considered 1, 3, 6, and 10 doping configurations for 1, 2, 3, and 4 Zn doped systems. (c) Calculated enthalpies of formation in various configurations with different numbers of Zn doping atoms.

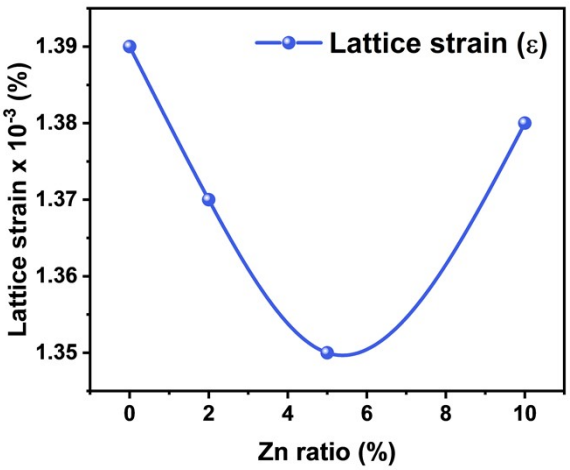

Figure S4. Lattice strain from Williamson-Hall plot.

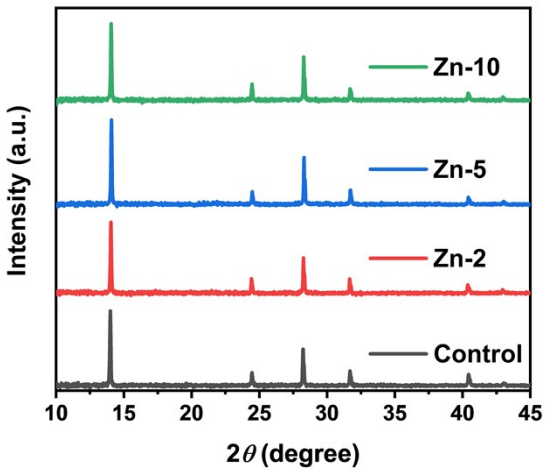

Figure S5. The full XRD patterns of Sn perovskite thin films with different concentrations of Zn metal powder.

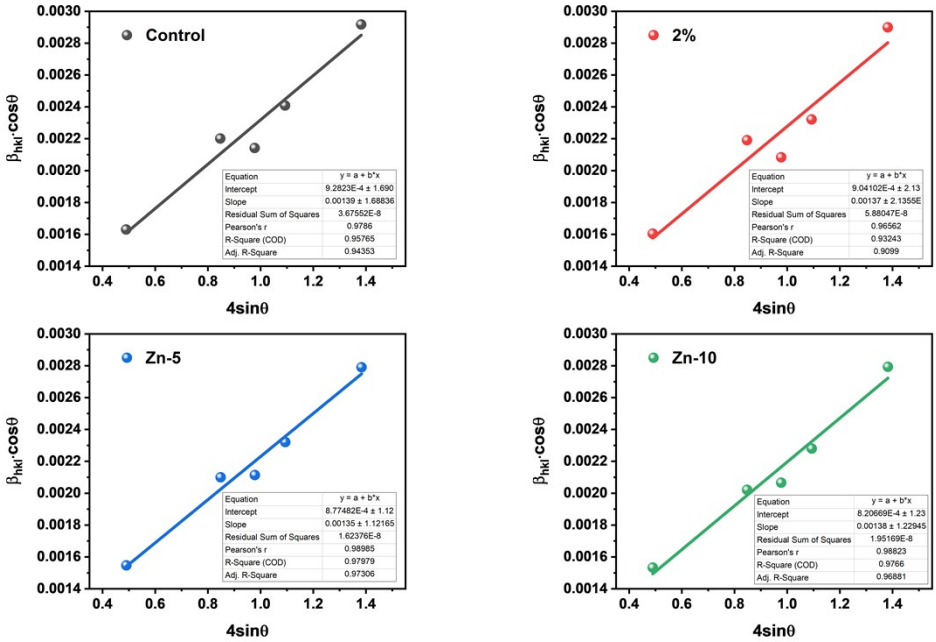

Figure S6. Williamson-Hall plots with different Zn ratios in Sn-based perovskite

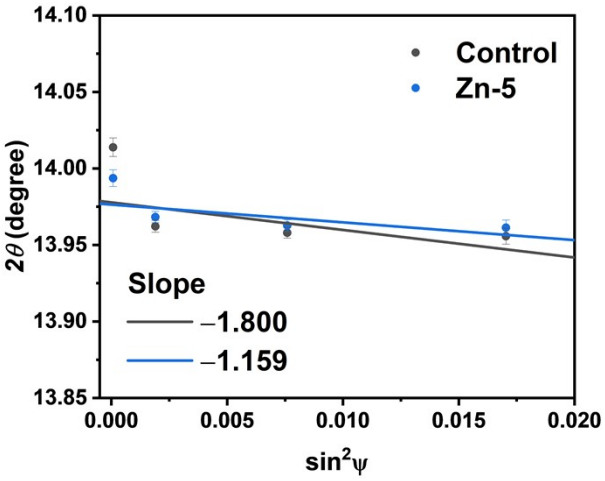

Figure S7. Residual strain distribution in the control and Zn-5 perovskite related to (100) plane (measured (points) and linear fitted (line) diffraction strain data as a function of $\sin^2\varphi$).

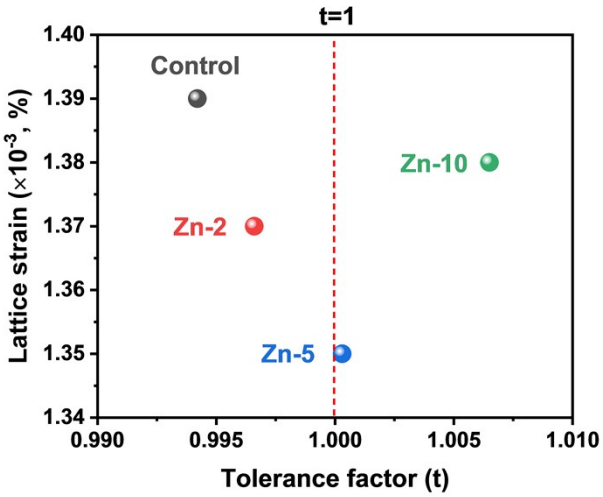

Figure S8. Relationship between the lattice strain and the tolerance factor (t) for various ratios of Zn-doped Sn perovskite.

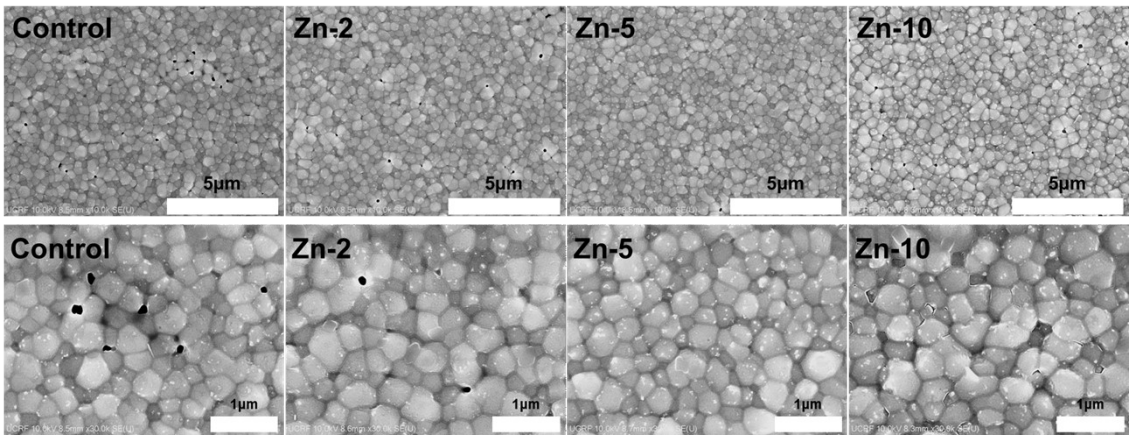

Figure S9. Surface SEM images of the perovskite films grown on PEDOT:PSS substrates by one-step process on a different ratio of Zn metal powder: 0%, 2%, 5%, and 10%; the scale bar is 5 μm. Corresponding the high-resolution SEM images of perovskite films; the scale bar is 1μm.

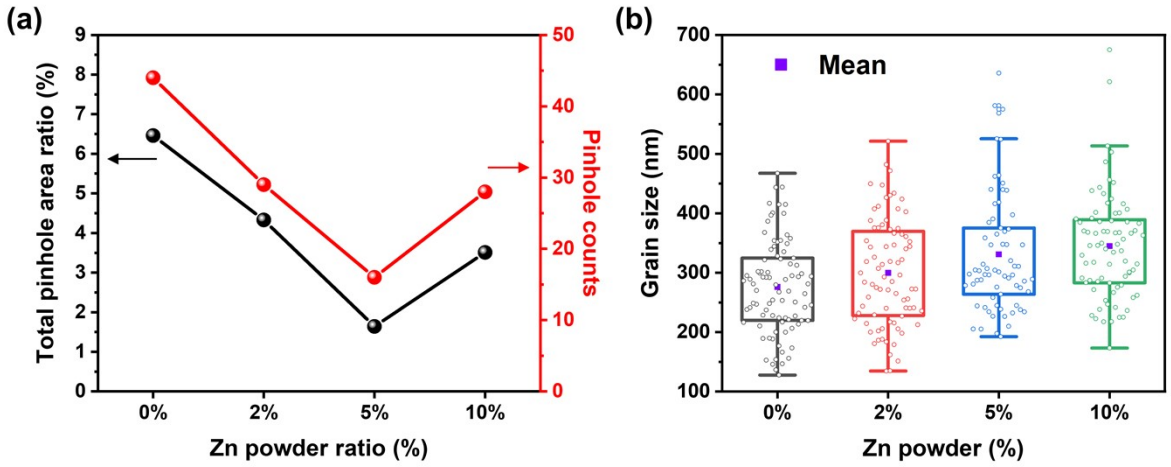

Figure S10. (a) Statistical analysis of total pinhole area ratio and pinhole counts per 120 μm^2 from the SEM images by ImageJ software and (b) calculated statistical distribution of grain size on Zn-doped Sn-based perovskite films.

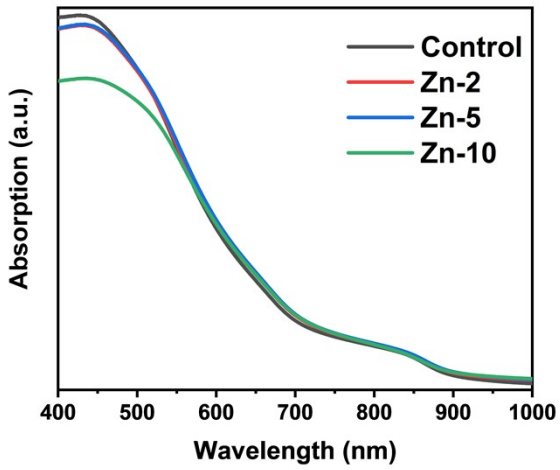

Figure S11. UV-vis absorption spectra of Sn-based perovskite thin films with different Zn ratios.

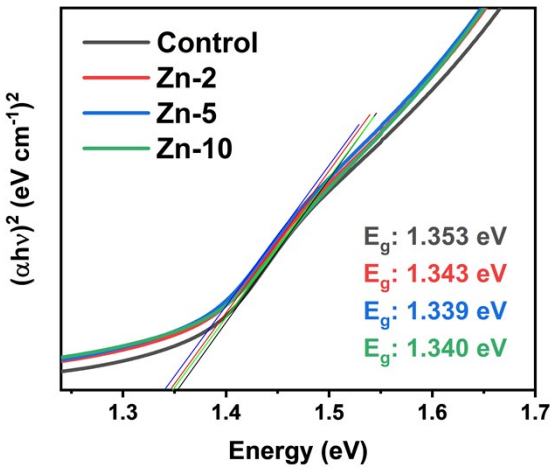

Figure S12. Tauc plot of Sn-based perovskite thin films with different Zn ratios.

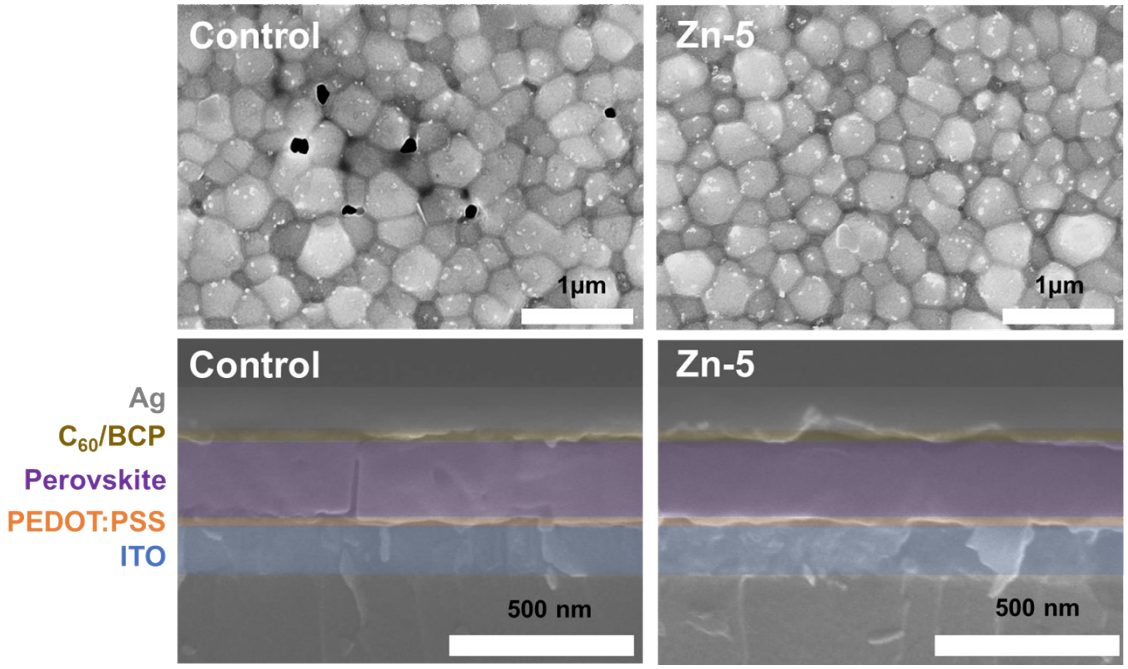

Figure S13. The surface and cross-sectional SEM images of Sn-based perovskite.

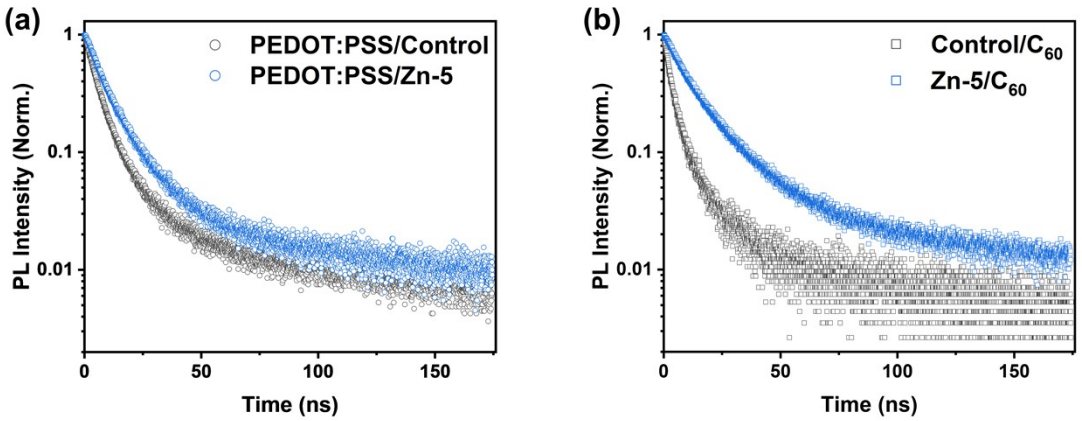

Figure S14. Time-resolved PL transients with quencher layers for control and Zn-5 films. (a) PEDOT:PSS is used for the hole quenching layer and (b) C_{60} for the electron quenching layer. Polymethyl methacrylate saves as a blocking layer to protect the perovskite films for measuring carrier lifetimes without the quenching layer in Figure 3c. We take the effective lifetime (τ) to calculate the carrier diffusion length with a bi-exponential function for fitting as in the previous report.[9]

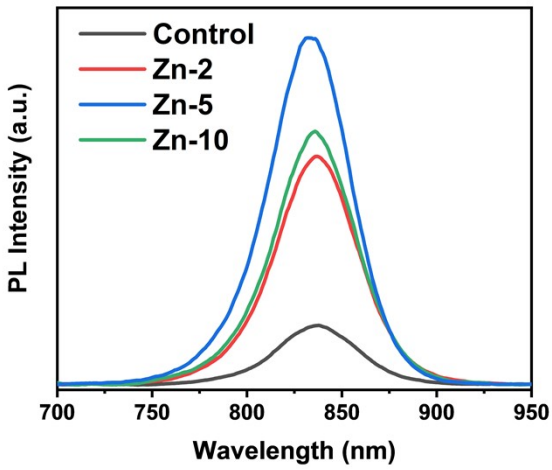

Figure S15. Steady-state photoluminescence spectra of Sn-based perovskite films deposited on glass.

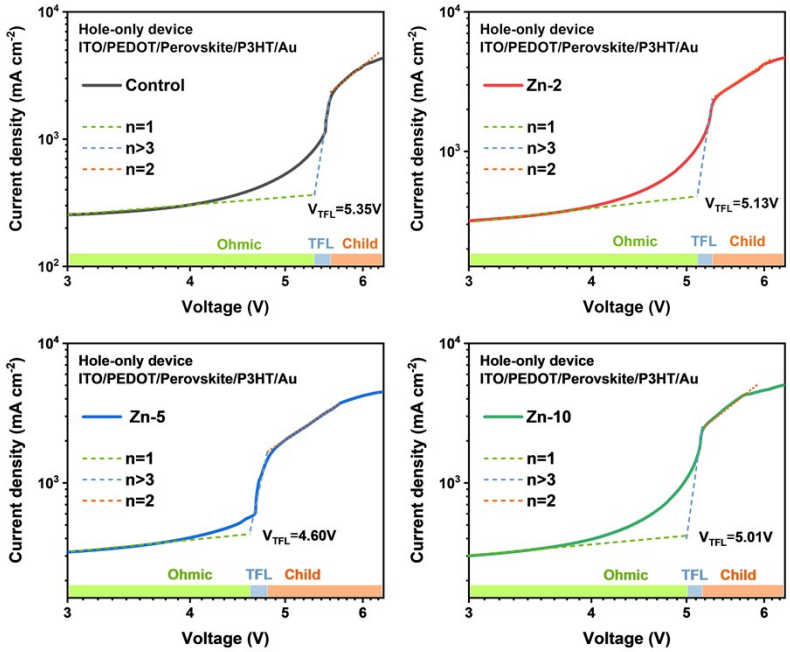

Figure S16. Space-charge-limited current measurement (SCLC) for hole-only devices (ITO/PEDOT:PSS/perovskite/P3HT/Au) based on different Zn ratio perovskite layers.

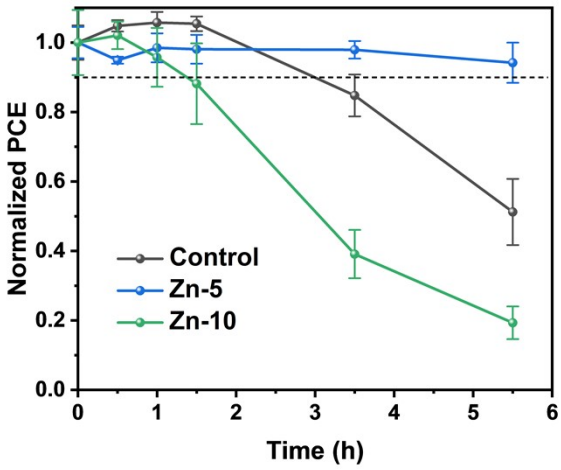

Figure S17. Stability of perovskite solar cells under ambient air (30% R.H. 25C°).

Table S1. The calculated d-spacing (lattice parameter), lattice strain, and average crystallite size of Zn-doped tin perovskite thin films.

Perovskite	d-spacing (100) [Å]	Lattice strain [%, x 10^{-3}]	Avg. crystallite size [nm]
Control	6.320	1.39 ± 0.168	772
Zn-2	6.301	1.37 ± 0.214	788
Zn-5	6.284	1.35 ± 0.112	826
Zn-10	6.292	1.38 ± 0.123	825

Table S2. Optimized lattice parameters (a, b, c) and volumes of $FASnI_3$ with different atomic percentage of Zn

Zn (at.%)	pristine	3.7	7.4	11.1	14.7
a ($Å^3$)	18.99	18.96	18.94	18.91	18.90
b ($Å^3$)	18.97	18.93	18.89	18.87	18.85
c ($Å^3$)	18.99	18.94	18.91	18.90	18.88
Volume ($Å^3$)	6841.45	6799.34	6764.89	6744.67	6726.61

Table S3. Tolerance factors calculated with different ratios of Zn^0 in $EDA_{0.01}FA_{0.98}SnI_3$.

$t = \frac{r_A + r_X}{\sqrt{2} \times (r_B + r_X)}$		$r_A = 0.01 \times r_{EDA^{2+}} + 0.98 \times r_{FA^+}$ $r_B = x \times r_{Zn^{2+}} + (1 - x) \times r_{Sn^{2+}}$		
Effective ionic radius	pm	Reference		
FA^+	253	Chem. Sci., 2015, 6, 3430-3433		
Sn^{2+}	115	Nano Energy 74 2020 104858 Shannon, R. D. Acta Cryst. A 1976, 32, 751-767		
I^-	220	Shannon, R. D. Acta Cryst. A 1976, 32, 751-767		
EDA^{2+}	305	Nano Energy 74 2020 104858		
Zn^{2+}	74	Shannon, R. D. Acta Cryst. A 1976, 32, 751-767		
Zn^0 ratios	**0**	**0.02**	**0.05**	**0.1**
rA	250.99	250.99	250.99	250.99
rB	115	114.18	112.95	110.9
rX	220	220	220	220
t	**0.99415**	**0.99659**	**1.00027**	**1.00647**

Table S4. The parameters of PL lifetime by fitting the TR-PL spectroscopy of Sn-based perovskite with different Zn^0 ratios.

Perovskite	τ_1 [ns]	A_1	τ_2 [ns]	A_2	R^2	τ_{avg} [ns]
Control	6.136	0.912	29.77	0.086	0.999	8.173
Zn-2	11.55	0.967	82.01	0.071	0.999	16.37
Zn-5	11.58	0.941	64.18	0.092	0.999	16.26
Zn-10	4.092	0.891	18.83	0.132	0.999	5.994

Table S5. Calculated current density, short-circuit current density (J_{SC}), open-circuit voltage (V_{OC}), fill factor (FF), and power conversion efficiency (PCE) values of Zn-doped Sn-based perovskite solar cells with different Zn^0 contents.

Perovskite	Cal. J_{SC} [mA cm^{-2}]	J_{SC} [mA cm^{-2}]	V_{OC} [V]	FF [%]	PCE [%]
Control	20.66	21.44	0.590	65.87	8.329
(Best& Avg.)		21.95 (20.44 ± 0.986)	0.583 (0.585 ± 0.015)	66.92 (68.28 ± 2.270)	8.560 (8.144 ± 0.191)
Zn-2	21.21	22.96	0.604	71.46	9.907
(Best& Avg.)		23.30 (23.04 ± 0.921)	0.620 (0.609 ± 0.012)	71.31 (68.40 ± 3.200)	10.30 (9.589 ± 0.372)
Zn-5	22.65	23.19	0.632	73.66	10.80
(Best& Avg.)		24.72 (23.89 ± 0.677)	0.649 (0.637 ± 0.010)	71.02 (70.74 ± 2.199)	11.39 (10.76 ± 0.255)
Zn-10	21.53	23.75	0.618	57.39	8.420
(Best& Avg.)		24.35 (23.35 ± 0.676)	0.549 (0.569 ± 0.026)	69.14 (65.06 ± 2.501)	9.250 (8.633 ± 0.292)

Table S6. Short-circuit current density (J_{SC}), open-circuit voltage (V_{OC}), fill factor (FF), power conversion efficiency (PCE), and hysteresis index values ($PCE_{reverse}$–$PCE_{forward}$)/$PCE_{reverse}$) of control and Zn-5 perovskite solar cells with different scan direction (forward from -0.1 V to 0.75 V and reverse from -0.75 V to 0.1 V).

Perovskite	Scan direction	J_{SC} [mA cm^{-2}]	V_{OC} [V]	FF [%]	PCE [%]	HI [%]
Control	Forward	21.79	0.531	64.92	7.510	13.98
	Reverse	21.95	0.583	66.92	8.559	
Zn-5	Forward	23.97	0.635	73.29	11.15	0.042
	Reverse	24.06	0.634	73.02	11.15	

Supplemental reference

1. M. D. Segall, P. J. D. Lindan, M. J. Probert, C. J. Pickard, P. J. Hasnip, S. J. Clark and M. C. Payne, *Journal of Physics: Condensed Matter*, 2002, **14**, 2717-2744.
2. J. P. Perdew and A. Zunger, *Physical Review B*, 1981, **23**, 5048-5079.
3. J. P. Perdew, K. Burke and Y. Wang, *Physical Review B*, 1996, **54**, 16533-16539.
4. D. Vanderbilt, *Physical Review B*, 1990, **41**, 7892-7895.
5. A. Tkatchenko and M. Scheffler, *Physical Review Letters*, 2009, **102**, 073005.
6. J. Barzilai and J. M. Borwein, *IMA Journal of Numerical Analysis*, 1988, **8**, 141-148.
7. H. J. Monkhorst and J. D. Pack, *Physical Review B*, 1976, **13**, 5188-5192.
8. J. Pascual, G. Nasti, M. H. Aldamasy, J. A. Smith, M. Flatken, N. Phung, D. Di Girolamo, S.-H. Turren-Cruz, M. Li, A. Dallmann, R. Avolio and A. Abate, *Materials Advances*, 2020, **1**, 1066-1070.
9. A. H. Proppe, R. Quintero-Bermudez, H. Tan, O. Voznyy, S. O. Kelley and E. H. Sargent, *Journal of the American Chemical Society*, 2018, **140**, 2890-2896.